Oceanic Origins of Historical Southwest Asia Precipitation During the Boreal Cold Season

ANDREW HOELL

Physical Sciences Division, NOAA/Earth System Research Laboratory, Boulder, Colorado

MATHEW BARLOW

Department of Environmental, Earth and Atmospheric Sciences, University of Massachusetts Lowell, Lowell, Massachusetts

FOREST CANNON[a]

Department of Geography, University of California Santa Barbara, Santa Barbara, California

TAIYI XU

Cooperative Institute for Research in the Environmental Sciences, University of Colorado, and Physical Sciences Division, NOAA/Earth System Research Laboratory, Boulder, Colorado

(Manuscript received 13 July 2016, in final form 21 November 2016)

ABSTRACT

While a strong influence on cold season southwest Asia precipitation by Pacific sea surface temperatures (SSTs) has been previously established, the scarcity of southwest Asia precipitation observations prior to 1960 renders the region's long-term precipitation history largely unknown. Here a large ensemble of atmospheric model simulations forced by observed time-varying boundary conditions for 1901–2012 is used to examine the long-term sensitivity of November–April southwest Asia precipitation to Pacific SSTs. It is first established that the models are able to reproduce the key features of regional variability during the best-observed 1960–2005 period and then the pre-1960 variability is investigated using the model simulations.

During the 1960–2005 period, both the mean precipitation and the two leading modes of precipitation variability during November–April are reasonably simulated by the atmospheric models, which include the previously identified relationships with El Niño–Southern Oscillation (ENSO) and the multidecadal warming of Indo-Pacific SSTs. Over the full 1901–2012 period, there are notable variations in precipitation and in the strength of the SST influence. A long-term drying of the region is associated with the Indo-Pacific warming, with a nearly 10% reduction in westernmost southwest Asia precipitation during 1938–2012. The influence of ENSO on southwest Asia precipitation varied in strength throughout the period: strong prior to the 1950s, weak between 1950 and 1980, and strongest after the 1980s. These variations were not antisymmetric between ENSO phases. El Niño was persistently related with anomalously wet conditions throughout 1901–2012, whereas La Niña was not closely linked to precipitation anomalies prior to the 1970s but has been associated with exceptionally dry conditions thereafter.

1. Introduction

The climate of southwest Asia, defined hereafter as the region bound by 25°–40°N, 40°–70°E (Fig. 1, blue box), during the November–April rainy season is closely related with sea surface temperature (SST) variations of the Pacific Ocean. The linkages between southwest Asia climate and SSTs were identified using model simulations forced by idealized SST patterns (Hoell et al. 2014a), analyses since 1950 using observed precipitation and atmospheric reanalyses (Barlow et al. 2002, 2015; Mariotti 2007; Hoell and Funk 2013; Hoell et al. 2013, 2014b, 2015a,b, 2017; Cannon et al. 2017), and atmospheric model simulations forced by time-varying boundary conditions since 1950 (Hoell et al. 2015a). Problematically, the sparse

[a] Current affiliation: Center for Western Weather and Water Extremes, Scripps Institution of Oceanography, University of California, San Diego, La Jolla, California.

Corresponding author e-mail: Andrew Hoell, andrew.hoell@noaa.gov

DOI: 10.1175/JCLI-D-16-0519.1

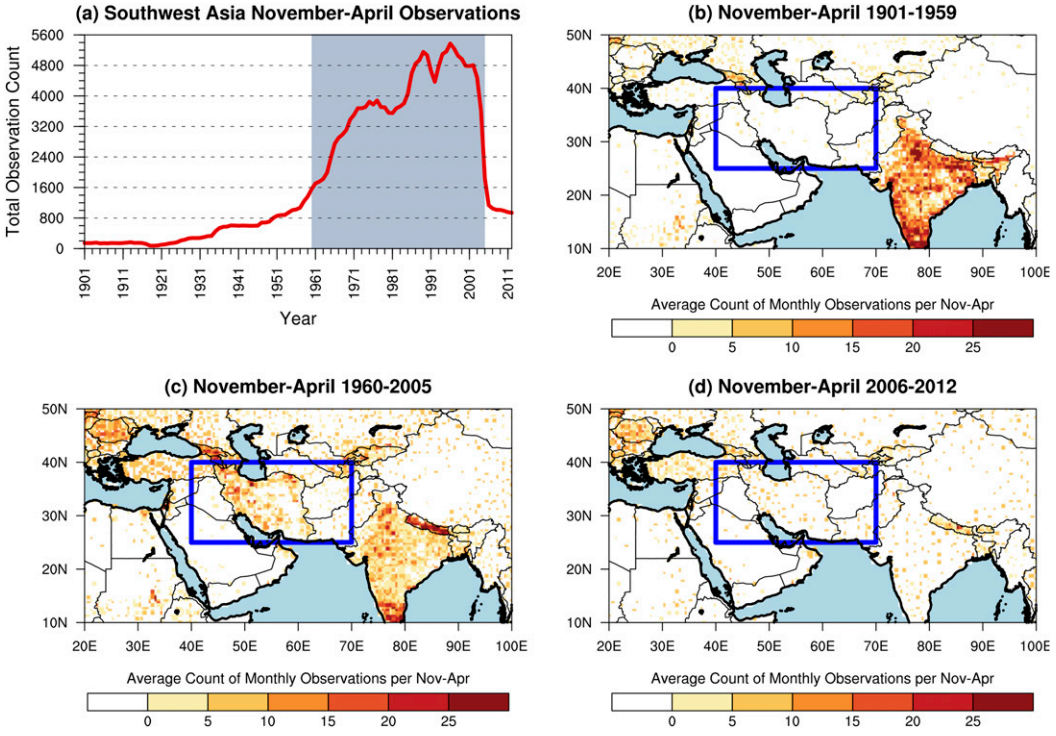

FIG. 1. (a) Total count of monthly precipitation observations contributing to each grid cell over southwest Asia for November–April of the labeled year in the GPCC precipitation dataset. Average count of monthly observations in each grid cell of the GPCC precipitation dataset per November–April season during (b) 1901–59, (c) 1960–2005, and (d) 2006–12. The blue box defines the region of southwest Asia.

precipitation gauge network before the 1960s across southwest Asia (Fig. 1) and the lack of satellite-guided precipitation estimates before the 1970s has prevented a more complete understanding of the long-term historical relationships between southwest Asia precipitation and SST. Therefore, in this study, we employ a large ensemble of atmospheric model simulations forced by observed time-varying boundary conditions during 1901–2012 to examine the historical relationships between SSTs and November–April southwest Asia precipitation.

There is considerable uncertainty in historical southwest Asia precipitation due to spatial and temporal inhomogeneity of precipitation observations throughout the region (Fig. 1; see also Hoell et al. 2014a). From 1901 to 1959, there were fewer than 800 total monthly precipitation observations across southwest Asia during each November–April (Fig. 1a), and those observations were widely scattered throughout the region (Fig. 1b). The time period in which southwest Asia precipitation was most abundantly sampled was 1960–2005; however, the year-to-year variations in precipitation sampling were large (Fig. 1a). Despite the relative abundance of precipitation observations during 1960–2005, the precipitation observations were taken primarily over Iran, so the fine spatial features of regional precipitation are likely unknown (Fig. 1c). From 2005 to 2012, precipitation sampling was reduced to levels as low as during 1940s (Fig. 1a). The uncertainty in historical southwest Asia precipitation therefore necessitates the use of atmospheric models to help diagnose the long-term relationships between SST and regional precipitation.

Pacific SSTs associated with El Niño–Southern Oscillation (ENSO) are closely related with November–April southwest Asia precipitation. The two phases of ENSO, El Niño and La Niña, are linked with anomalous equivalent barotropic Rossby waves over southwest Asia that in turn modify the regional precipitation (Mariotti 2007; Hoell and Funk 2013; Hoell et al. 2013, 2014b, 2015a). During La Niña, on average, anomalous high pressure prevails over southwest Asia. The high pressure over southwest Asia during La Niña interacts with the mean middle- and upper-level tropospheric jet, thereby producing midtropospheric cold temperature advection that results in precipitation-reducing anomalous subsidence. The high pressure over southwest Asia during La Niña also reduces the climatological vertically integrated moisture fluxes and convergence into the region, which further reduces the regional precipitation. During El Niño, on average, anomalous low pressure prevails over southwest Asia. The low pressure over

southwest Asia during El Niño interacts with the mean middle- and upper-level tropospheric jet, thereby producing midtropospheric warm temperature advection that results in precipitation-enhancing anomalous ascent. The low pressure over southwest Asia during El Niño also enhances the climatological vertically integrated moisture fluxes and convergence into the region, which further enhances the regional precipitation.

La Niña events have occurred simultaneously with the strongest November–April southwest Asia droughts post-1980 (Barlow et al. 2002; Hoell and Funk 2013; Hoell et al. 2014a, 2015a, 2017). As a result, the most recent studies on the relationship between ENSO and southwest Asia climate have focused on La Niña. These most recent studies found that the strongest southwest Asia droughts occurred simultaneously with a warm tropical western Pacific Ocean and a cool tropical central Pacific Ocean separated by a sharp gradient in SST between 150°E and the date line. All but one of these studies were solely observational analyses, with Hoell et al. (2015a) using a 10-member ensemble of atmospheric model simulations forced by prescribed time-varying boundary conditions since 1950. This collection of studies is therefore largely unable to fully demonstrate causality or sensitivity of southwest Asia climate to SST during La Niña due to the many additional influences on regional precipitation on intraseasonal to seasonal time scales, such as the Madden–Julian oscillation (Barlow et al. 2005; Nazemosadat and Ghaedamini 2010; Hoell et al. 2013) and the North Atlantic Oscillation (Cullen and deMenocal 2000; Aizen et al. 2001; Cullen et al. 2002; Krichak et al. 2002; Mann 2002; Syed et al. 2006). Furthermore, these studies primarily focused on a short time period, so it is unclear from these analyses whether the relationships between La Niña and southwest Asia precipitation have changed through time. Therefore, in this study, we use a large ensemble of atmospheric model simulations during 1901–2012 to examine the sensitivity of southwest Asia climate to SST during La Niña events and whether this sensitivity has changed through time. We also examine the sensitivity of historical southwest Asia climate to SST during El Niño, which has been understudied.

Results from atmospheric model experiments forced by idealized SST patterns reveal that a pattern similar to the long-term SST change has a drying effect on southwest Asia (Hoell et al. 2014a). The long-term SST change pattern used to force the models examined by Hoell et al. (2014a) features a warm Indo-western Pacific Ocean and a cool central and eastern Pacific Ocean [see Fig. 1 in Schubert et al. (2009)], which resemble an SST pattern similar to the long-term change in observed SST during the twentieth century when ENSO is removed (e.g., Solomon and Newman 2012; Compo and Sardeshmukh 2010). Therefore, we examine whether a drying of southwest Asia climate has occurred in the region's long-term precipitation history, and whether that drying is related with SST, using the large ensemble of atmospheric model simulations forced by time-varying boundary conditions.

The goal of this study is to better understand the historical sensitivity of November–April southwest Asia precipitation to Pacific SST patterns and their variations. We employ a 43-member ensemble of atmospheric model simulations from three separate models forced by time-varying boundary conditions during 1901–2012. In section 3, we assess whether the three atmospheric models adequately reproduce southwest Asia precipitation during 1960–2005, the period in which southwest Asia precipitation observations were most abundant. Specifically, we address whether the atmospheric models capture the regional precipitation climatology, the leading modes of regional precipitation and their relationships with SSTs, and the temporal variability of the regional precipitation. In section 4, we assess the relationships among El Niño, La Niña, and southwest Asia precipitation, and how those relationships have changed between 1901 and 2012. Also in section 4, we assess the long-term changes in southwest Asia precipitation and whether the long-term changes are related with SSTs. In section 5, we provide a summary and a brief discussion on this significance of this work and its implications for future studies.

2. Data and methods

a. Observed data and atmospheric reanalyses

An estimate of observed precipitation on a 0.5° × 0.5° fixed latitude–longitude grid is drawn from the land-only Global Precipitation Climatology Centre (GPCC) monthly precipitation dataset version 7 (Schneider et al. 2014).

An estimate of observed SSTs on a fixed 1° × 1° latitude–longitude grid is drawn from Hurrell et al. (2008). These SSTs also prescribe the SST and sea ice concentration boundary conditions in the atmospheric model simulations. Hurrell et al. (2008) constructs this SST dataset by merging the Hadley Centre Sea Ice and SST (HadISST) and NOAA weekly optimum interpolation (OI) datasets. The merging procedure used to construct the Hurrell et al. (2008) dataset takes advantage of the higher-resolution SST of the NOAA weekly OI datasets.

An estimate of the observed 200-hPa geopotential height on a 2° × 2° fixed latitude–longitude grid is drawn from the Twentieth Century Reanalysis (20CR), version 2c (Compo et al. 2011). The 20CR version 2c is constructed from available daily surface pressure observations, monthly

TABLE 1. Description of atmospheric models.

	CAM5	GEOS-5	AM3
Developing modeling center	National Center for Atmospheric Research	National Aeronautics and Space Administration	Geophysical Fluid Dynamics Laboratory
Model reference(s)	Neale et al. (2012)	Molod et al. (2012) Schubert et al. (2014)	Donner et al. (2011)
No. of members	14	12	17
Horizontal resolution	1.0° × 0.75°	1.25° × 1.1°	1.9° × 1.9°
Levels	25	72	48
SST and sea ice concentrations	Hurrell et al. (2008)	Hurrell et al. (2008)	Hurrell et al. (2008)
Pre-2006 greenhouse gas ozone aerosols	Lamarque et al. (2010)	Lamarque et al. (2010)	Lamarque et al. (2010)
Post-2006 greenhouse gas	Meinshausen et al. (2011) (RCP6)	Meinshausen et al. (2011) (RCP6)	Meinshausen et al. (2011) (RCP4.5)
Post-2006 ozone aerosols	Lamarque et al. (2011)	Lamarque et al. (2011)	Lamarque et al. (2011)

observed SST, and monthly observed sea ice concentrations for 1871 to the near present. The 20CR version 2c utilizes an ensemble Kalman filter assimilation and an ensemble of forecasts from a weather prediction model. The 20CR compares very closely in terms of Northern Hemisphere upper-tropospheric circulation during the cold season with other modern reanalyses, such as the ERA-40 and NCEP–NCAR reanalyses, during their common periods [see Fig. 15 in Compo et al. (2011)].

b. *Atmospheric model simulations forced by observed boundary conditions*

Southwest Asia climate during 1901–2012 is examined using a 43-member ensemble of atmospheric model simulations forced by observed time-varying boundary conditions: SST, sea ice concentrations, greenhouse gases, and ozone. Three atmospheric models are used in this study: 1) 14 members from the Community Atmosphere Model, version 5 (CAM5; Neale et al. 2012), developed by the National Center for Atmospheric Research (NCAR), 2) 12 members from the Goddard Earth Observing System Model, version 5 (GEOS-5; Molod et al. 2012), developed by the Global Modeling and Assimilation Office of the National Aeronautics and Space Administration (NASA), and 3) 17 members from the Atmosphere Model, version 3 (AM3; Donner et al. 2011), developed by the Geophysical Fluid Dynamics Laboratory (GFDL). Each ensemble member has different weather variability owing to their initialization from different atmospheric states. Outputs from each model were interpolated to the CAM5 grid for analysis. All 43 ensemble members across the three separate models are aggregated to create a single multimodel ensemble in which each member is weighted equally with the purpose of creating as large of an ensemble size as possible. The aggregation is justified through comparisons of individual model simulations described in section 3. A description of the three atmospheric models and the boundary conditions used to drive the models are provided in Table 1. Further documentation and outputs from the atmospheric model experiments can be found online at http://www.esrl.noaa.gov/psd/repository/alias/facts.

c. *Principal components of southwest Asia precipitation*

Principal component analysis is used to identify the leading two modes of November–April southwest Asia precipitation in models and observations. We calculate the area-weighted principal components of November–April average precipitation anomalies over the region defined as southwest Asia (25°–40°N, 40°–70°E) for 1960–2005. The spatial precipitation patterns related with the leading principal components of southwest Asia precipitation are identified through a temporal correlation of the principal components with precipitation anomalies at each grid point.

3. Comparison of observed and simulated southwest Asia precipitation

We compare observed and simulated precipitation for 1960–2005, the period in which regional precipitation observations were most abundant (Fig. 1), to verify that the atmospheric models can simulate southwest Asia precipitation adequately. The atmospheric models simulate November–April southwest Asia precipitation well in both time and space. The atmospheric models simulate November–April southwest Asia 1960–2005 precipitation

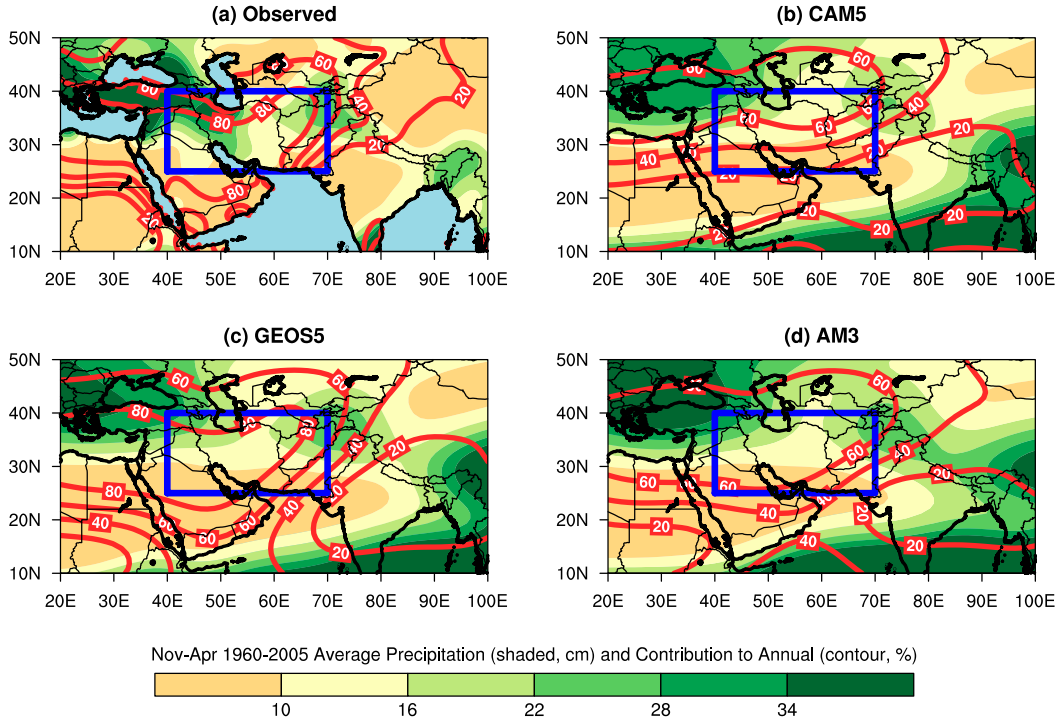

FIG. 2. November–April 1960–2005 average precipitation and percent contribution to the annual average in (a) observation, (b) CAM5, (c) GEOS-5, and (d) AM3.

well in terms of precipitation means (Fig. 2), the leading patterns of precipitation variability (Figs. 3 and 4), the global SST and atmospheric circulation patterns associated with the leading patterns of precipitation variability (Figs. 5 and 6), and temporal precipitation variability (Fig. 8).

To first order, the atmospheric models reproduce the mean November–April 1960–2005 spatial southwest Asia precipitation (Fig. 2). The greatest precipitation amounts in observations and models fall to the west of the region's high mountains and the lowest over the region's low elevations. Each of the models simulate the mean November–April upper-tropospheric jet farther to the north than in observations (not shown), which shifts the models' seasonal precipitation maximum north of 35°N and the models' seasonal precipitation minimum into the southern extent of southwest Asia. Each of the atmospheric models would be incapable of capturing the local-scale southwest Asia precipitation features, even if those precipitation features were well understood in observations (Fig. 1c), because of the coarse resolution of the models relative to the spatial scales of the region's topographical variations. For example, the models' dry bias over the Zagros Mountains in Iran and the models' wet bias over the Karakum Desert lowlands in Turkmenistan could be explained by the models' inability to capture local-scale topographic interactions.

The models reproduce the leading modes of observed November–April 1960–2005 southwest Asia precipitation variability. The leading modes of simulated and observed precipitation variability are compared through an examination of the spatial precipitation patterns related with the leading two principal components of southwest Asia precipitation (Figs. 3 and 4). The leading two principal components of observed southwest Asia precipitation explain 42% of the total variance, and project on to patterns of uniform regional precipitation changes and a precipitation dipole between the western and eastern areas of the region, respectively (Figs. 3a,c). The leading two principal components of simulated southwest Asia precipitation from one member of each model projects on to qualitatively the same patterns as in observations (cf. Figs. 4 and 3a,c). The leading precipitation principal components in one simulation of each model are analogous to the leading precipitation principal components in observations, since both contain a mixture of atmospheric and boundary condition-forced variability. The leading two principal components of the simulated ensemble mean precipitation also project on to the same patterns as in observations and the individual model simulations (cf. Figs 3b,d, Figs. 3a,b, and Fig. 4). Principal component analysis on the simulated ensemble mean precipitation mutes internal atmospheric variability and highlights the variability forced by the prescribed boundary conditions since the prescribed boundary conditions are the same across each simulation. As a result, the leading principal

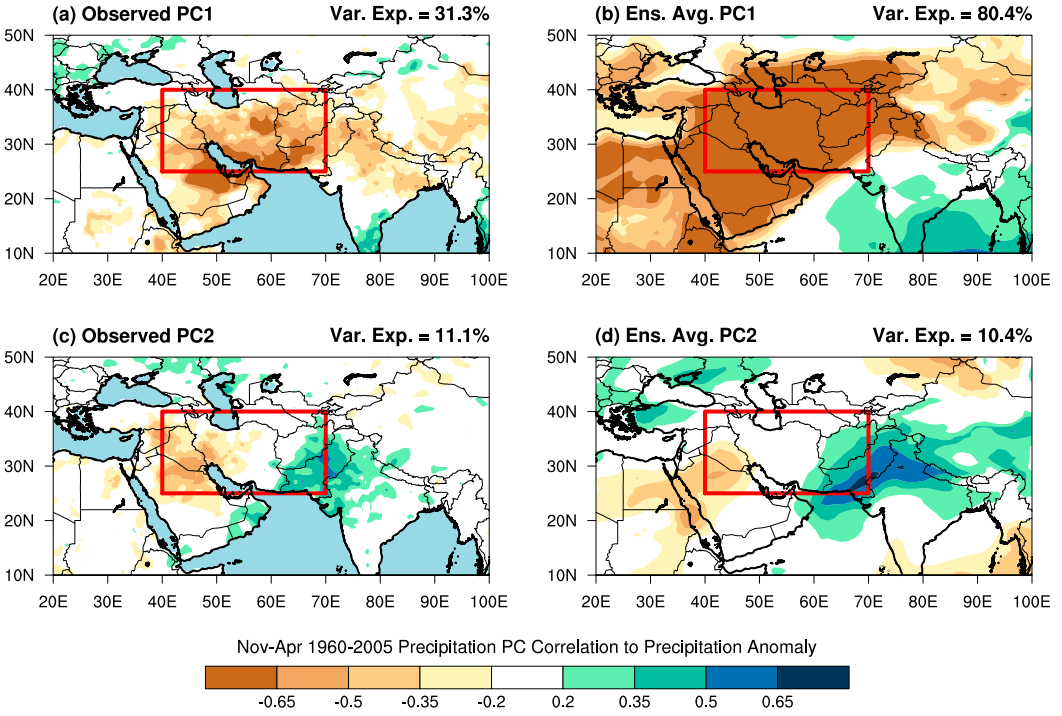

FIG. 3. November–April 1960–2005 correlation of the (a),(b) first and (c),(d) second principal components of southwest Asia precipitation and precipitation anomaly in (left) observations and (right) the simulated ensemble average. Correlations are significant at $p < 0.10$. Significance is calculated using the two-sided Student's t test.

component of ensemble average precipitation explains 80% of the variance. The similarities of the simulated ensemble mean, individual ensemble members from each model, and observed precipitation principal components thereby indicate that the leading modes of southwest Asia precipitation variability are closely related to the time-varying boundary conditions.

The simulated ensemble members and simulated ensemble mean reproduce the observed relationships between the leading patterns of November–April 1960–2005

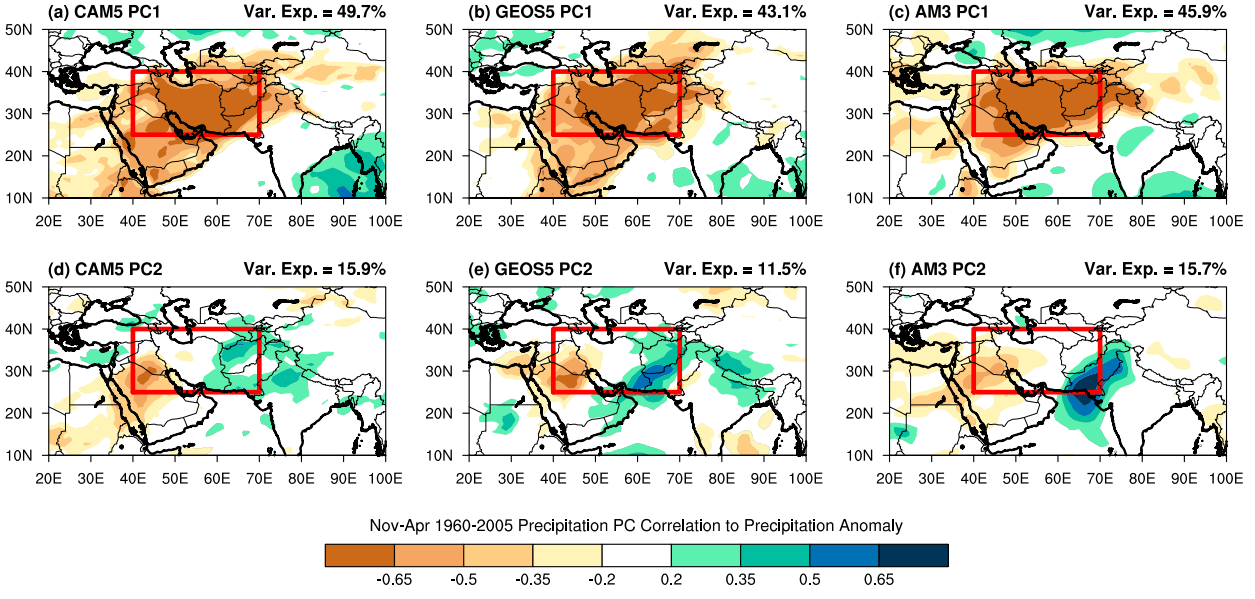

FIG. 4. As in Fig. 3, but for the first member of (a),(d) CAM5, (b),(e) GEOS-5, and (c),(f) AM3 model ensembles.

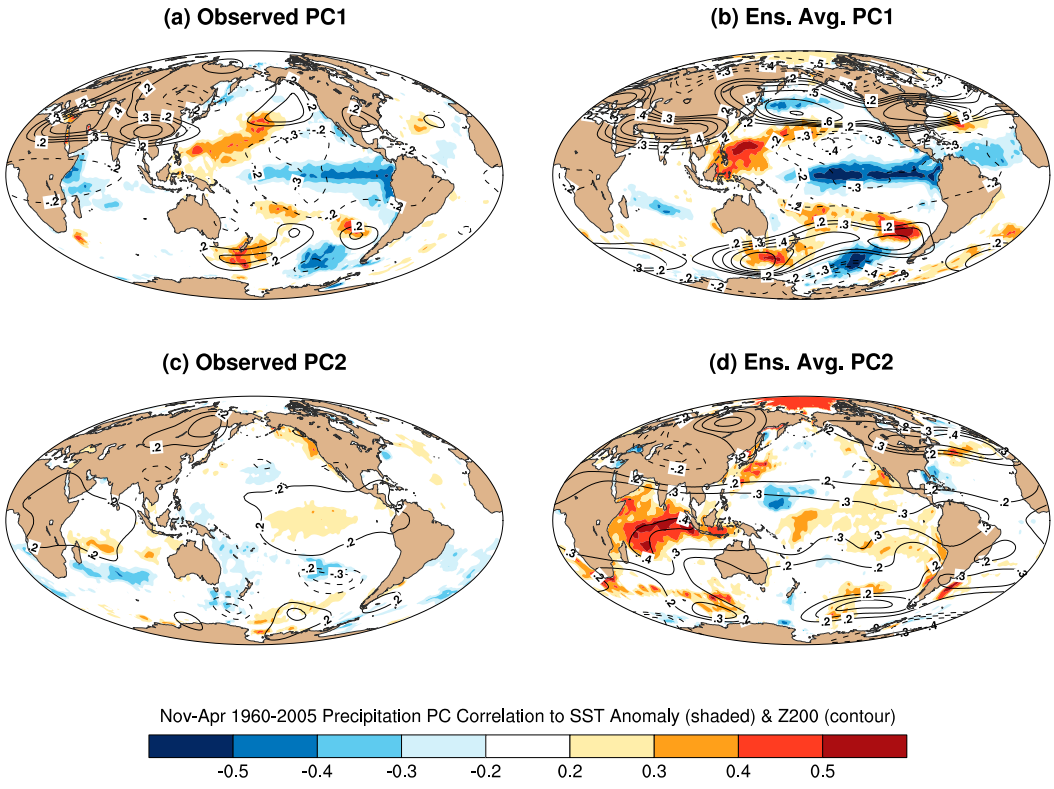

FIG. 5. November–April 1960–2005 correlation of the (a),(b) first and (c),(d) second principal components of southwest Asia precipitation and SST anomaly and 200-hPa geopotential height anomaly in (left) observations and reanalyses and (right) the simulated ensemble average. Correlations are significant at $p < 0.10$. Significance is calculated using the two-sided Student's t test.

southwest Asia precipitation variability, 200-hPa geopotential height, and SST anomalies. The leading principal component of southwest Asia precipitation in observation (Fig. 5a), individual model simulations (Figs. 6a–c), and the simulated ensemble mean (Fig. 5b) are related with global SST and 200-hPa geopotential heights similar to those that occur during ENSO. Internal atmospheric variability between observations and the model ensemble members is the reason for differences in the strength and pattern of global SST and 200-hPa geopotential height relationships with southwest Asia precipitation. Likewise, the strongest correlations between SST and 200-hPa geopotential heights are related with the simulated ensemble mean southwest Asia precipitation since internal atmospheric variability is muted, thus highlighting the role of the prescribed boundary conditions.

The leading principal component of southwest Asia precipitation is not closely related with ENSO-like decadal variability. First, the SST patterns related to the leading principal component of southwest Asia in model simulations and observations are related only to tropical eastern Pacific SSTs, which contrasts the clearly defined tropical and extratropical eastern Pacific SST loadings characteristic of ENSO-like decadal variability [see Fig. 2 in Mantua et al. (1997) and Fig. 1 in Dai (2013)]. Second, the simulated ensemble average precipitation, which highlights the effects of SSTs, does not demonstrate consistent precipitation anomaly patterns between positive and negative periods of ENSO-like decadal variability defined by Dai (2013) during the twentieth century (Fig. 7). In fact, the simulated precipitation composites during positive and negative periods of decadal variability share similarities with the precipitation pattern of the second principal component of southwest Asia (Figs. 3 and 4), which we show in the following to be unrelated with ENSO-like decadal variability.

The second principal component of southwest Asia precipitation is related to warming of the Indian and Pacific Oceans and 200-hPa geopotential height increases in observation (Fig. 5c), individual model simulations (Figs. 6d–f), and the simulated ensemble mean (Fig. 5d). These relationships are much stronger in the simulated ensemble mean than in observations and the individual model simulations due to the prominent effect of the boundary conditions. These results indicate that the relationship between southwest Asia

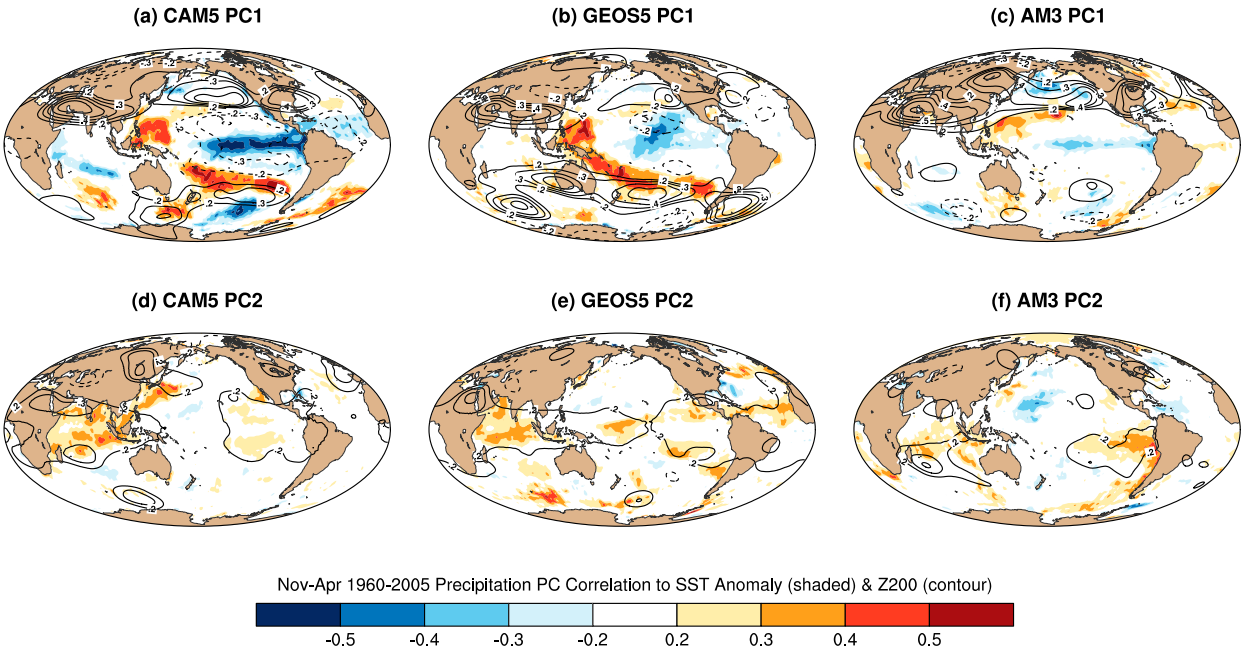

FIG. 6. As in Fig. 5, but for the first member of (a),(d) CAM5, (b),(e) GEOS-5, and (c),(f) AM3 model ensembles.

precipitation and the boundary conditions is primarily driven by SSTs.

The models capture the observed temporal precipitation variability of southwest Asia during November–April 1960–2005 (Figs. 8 and 9). The simulated ensemble mean precipitation variability tracks closely with observations (Fig. 8), as evidenced by 30-yr end point correlations between the simulated ensemble mean precipitation and observed precipitation in the early 2000s of greater than 0.70 (Fig. 9, blue line). The observed southwest Asia precipitation falls within the 43-member simulated ensemble spread during 1960–2005 (Fig. 8). By contrast, the models do not capture the best estimate of observed southwest Asia precipitation prior to the 1960s (Figs. 8 and 9), the time period in which regional precipitation observations were spatially and temporally scarce (Fig. 1). The 30-yr end point correlation between the simulated ensemble average and observed southwest Asia precipitation ranges between −0.2 and 0.2 prior to the 1990s (Fig. 9, blue line).

The significant correlations between the simulated ensemble mean and observed southwest Asia precipitation during 1960–2005 are primarily caused by a better representation of observed southwest Asia precipitation through improved sampling and not a change in the regional precipitation sensitivity to the prescribed boundary conditions. The temporal sensitivity of southwest Asia precipitation to the prescribed boundary conditions is tested through an examination of the correlation between each member of the simulated ensemble and the simulated ensemble mean. This method allows one to test how individual realizations of the simulated climate compare with a simulated climate that responds primarily to the prescribed boundary conditions. The average of the 30-yr end point correlations (Fig. 9, black line) between the simulated ensembles and the simulated ensemble average is consistent through 1901–2012, ranging between 0.45 and 0.60. Since southwest Asia precipitation sensitivity to the prescribed boundary conditions is consistent through time, atmospheric models driven by prescribed boundary conditions are therefore appropriate tools to examine the historical relationships between SSTs and the region's climate variability.

4. Historical southwest Asia precipitation and SST

The leading modes of November–April southwest Asia precipitation are closely related with the boundary conditions prescribed in the atmospheric model simulations. The close relationships between the prescribed boundary conditions and southwest Asia precipitation are primarily a result of SSTs, as evidenced by significant correlations between the leading modes of southwest Asia precipitation and Indian and Pacific Ocean SST anomalies (Figs. 5 and 6). We therefore examine the historical relationship between southwest Asia climate and SSTs during November–April 1901–2012 using the 43-member ensemble of atmospheric model simulations driven by prescribed boundary conditions. We focus on two modes of SST variability that have been identified

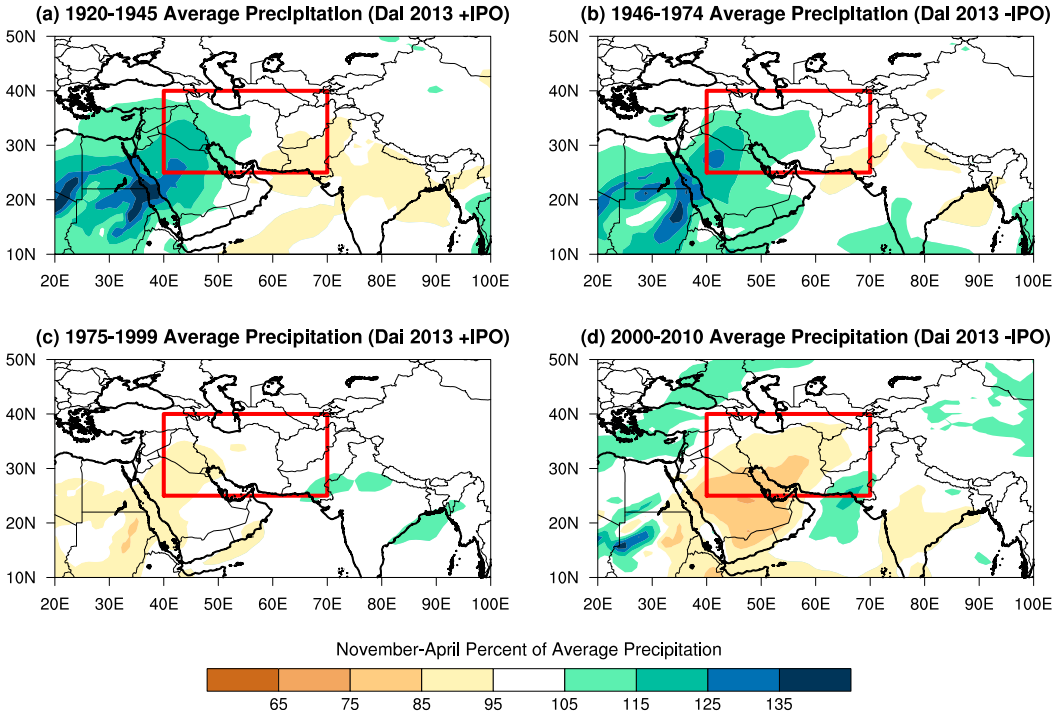

FIG. 7. November–April simulated ensemble average percent of average precipitation during (a) 1920–45, (b) 1946–74, (c) 1975–99, and (d) 2000–2010. These time periods correspond with positive and negative ENSO-like decadal variability epochs defined by Dai (2013), which Dai (2013) refers to as the interdecadal Pacific oscillation (IPO).

herein (Figs. 5 and 6) and previously as important drivers of southwest Asia precipitation: ENSO (Mariotti 2007; Hoell and Funk 2013; Hoell et al. 2013, 2014b, 2015a) and the long-term warming of the Indian and Pacific Oceans (Hoell et al. 2014a). This analysis would be impossible using observations alone because of the region's poor historical observational record prior to the 1960s (Fig. 1).

a. ENSO

Observations (Fig. 5a), individual simulations from each model (Figs. 6a–c), and the simulated ensemble mean across multiple models (Fig. 5b) all show that the leading principal component of November–April southwest Asia precipitation is related to SST anomalies associated with ENSO. The strength of the relationship between ENSO and southwest Asia precipitation varies throughout 1901–2012 (Fig. 10). The temporal relationship between southwest Asia precipitation and ENSO is tested through an examination of the 30-yr end point correlations of precipitation in the 43 simulated ensemble members with Niño-3.4 index (Fig. 10, black dots). The Niño-3.4 index is defined as the areally averaged SST anomaly over the region 5°S–5°N, 170°–120°W. This examination allows one to understand how precipitation in an individual realization of the simulated climate, which includes the effects of internal atmospheric variability, varies simultaneously with ENSO. The average of the 30-yr end point correlations between the 43 simulated ensemble members and the Niño-3.4 index (Fig. 10, black line) demonstrates extensive variation throughout 1901–2012; ranging from 0.3 prior to the 1950s, to 0.10 in the 1970s, and to 0.50 in the early 2000s. The relationship between the Niño-3.4 index and the simulated ensemble average southwest Asia precipitation, which reflects the sensitivity of the regional precipitation when internal atmospheric variability is muted, also demonstrates similar behavior in time, except with higher correlations (Fig. 10, red line). The 30-yr end point correlations between the Niño-3.4 index and observed southwest Asia precipitation also demonstrate similar behavior in the latter part of the twentieth century, but the scarcity of historical observations renders this analysis unreliable in a historical context (Fig. 10, blue line).

We are therefore motivated to assess the temporal changes in the relationship between ENSO and November–April 1901–2012 southwest Asia climate during the two phases of ENSO, El Niño and La Niña, using the ensemble of atmospheric model simulations. Temporal changes are assessed through analyses of three time periods of nearly equal length (1901–37, 1938–74, and 1975–2012) when the

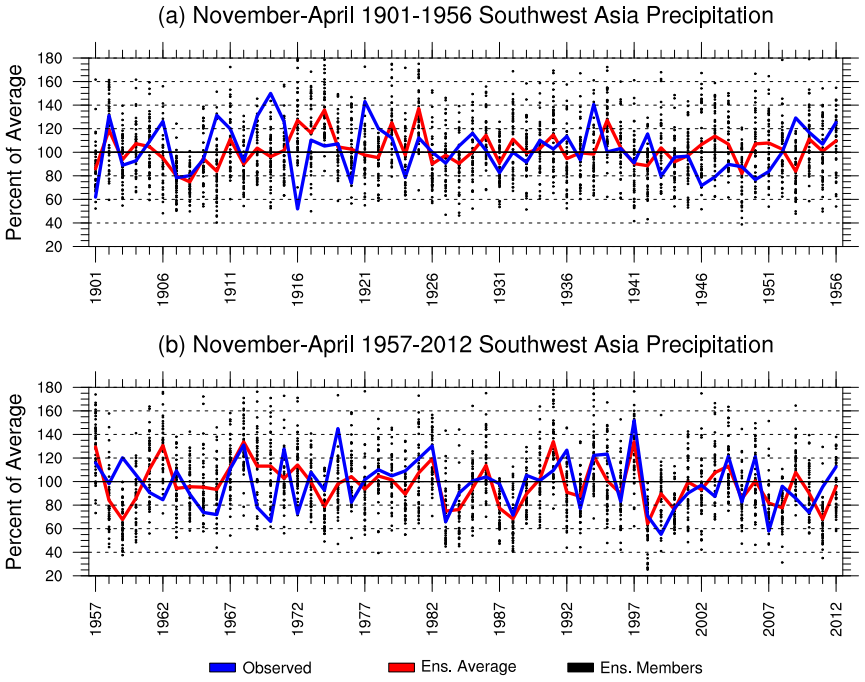

FIG. 8. November–April areally averaged percent of average southwest Asia precipitation resolved by observations (blue line), the simulated ensemble average (red line), and the simulated ensemble members (black dots).

Niño-3.4 index exceeds 0.5°C (El Niño) or falls below −0.5°C (La Niña). These three roughly 36-yr time periods are analyzed to provide a large enough sample size in which to track the changing relationships between SSTs and southwest Asia precipitation. Further, the last period almost entirely overlaps with the satellite era. The El Niño and La Niña years are listed in Table 2. Southwest Asia climate is examined in terms of spatial precipitation and probability density functions (PDFs) of areally averaged regional precipitation. The 200-hPa geopotential height and SST anomalies are also analyzed to provide a first-order diagnosis of potential drivers of southwest Asia precipitation. Results are displayed as changes relative to ENSO neutral, defined as 1901–2012 November–April seasons in which the Niño-3.4 index falls between −0.5° and 0.5°C. An ENSO neutral baseline is used in order to neglect the potential biases that El Niño or La Niña may introduce.

La Niña is on average related with materially different patterns of November–April southwest Asia precipitation across 1901–37, 1938–74, and 1975–2012 (Fig. 11). The variable behavior of southwest Asia precipitation during La Niña across the three time periods considered helps to explain the poor correlations between the Niño-3.4 index and southwest Asia precipitation prior to the 1970s (Fig. 10). The 1975–2012 La Niña events are related to statistically significant regionwide southwest Asia precipitation deficits relative to ENSO neutral conditions (Figs. 11a) of a similar pattern and magnitude as the observed precipitation anomalies during the same time period (Hoell et al. 2015a). The strongest precipitation deficits throughout southwest Asia during 1975–2012 La Niña are simulated over the western portions of the region with values that fall below 75% of ENSO neutral (Fig. 11a). The PDF of southwest Asia precipitation during 1975–2012 La Niña periods indicates a shift of the entire precipitation distribution by about 20% to drier conditions relative to ENSO neutral (Fig. 11b). The spread of the southwest Asia precipitation PDF during 1975–2012 La Niña is nearly as broad as ENSO neutral conditions, which reflects the importance of internal atmospheric variability to the region even in the presence of a strongly forced SST signal during La Niña. The narrowing spread, however, implies that internal atmospheric variability may not be as important during these La Niña periods.

By contrast, 1938–74 and 1901–37 La Niñas are unrelated to regionwide southwest Asia precipitation changes relative to ENSO neutral (Figs. 11c–f). La Niña events during these two periods are related with relatively weak southwest Asia precipitation increases only south of 35°N in comparison with 1975–2012 La Niña (Fig. 11). The southwest Asia La Niña precipitation PDFs during 1938–74 and 1901–37 are virtually

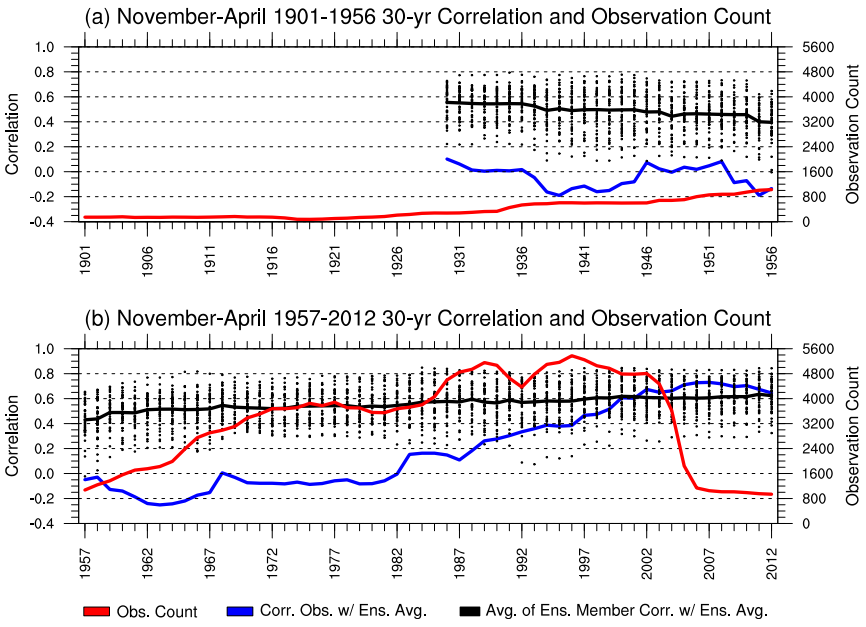

FIG. 9. November–April areally averaged southwest Asia 30-yr end point correlation of observed and simulated ensemble average precipitation (blue line), simulated ensemble members with the simulated ensemble average precipitation (dots), and average of the simulated ensemble members with the simulated ensemble average precipitation (black line). Total number of monthly precipitation observations over southwest Asia during November–April of the labeled year (red line; see also Fig. 1a).

indistinguishable from the ENSO neutral precipitation PDFs (Figs. 11d,f) in terms of the SST-forced signal and contributions from internal atmospheric variability.

The stark differences in southwest Asia precipitation for La Niñas of 1975–2012, 1938–74, and 1901–37 are related to different global atmospheric circulation and SST anomalies (Fig. 12). The differences in 200-hPa geopotential height and SST anomalies highlight important large-scale mechanisms responsible for southwest Asia precipitation. SST anomalies during La Niña of 1975–2012 are characterized by a sharp contrast between the central and western tropical Pacific Ocean in excess of 1.5°C (Figs. 12a,b). The sharp SST anomaly contrast between the central and western tropical Pacific Ocean is a result of the greater rate of observed warming over the Indo-western Pacific Ocean relative to the central Pacific Ocean (e.g., Compo and Sardeshmukh 2010; Solomon and Newman 2012). There is considerable structure to the Northern Hemisphere 200-hPa geopotential height anomaly field during 1975–2012 La Niña, highlighted by strong anomalies and gradients over the North Pacific, North America, and southern Asia, which demonstrate striking resemblance to observed conditions during La Niña events since the 1980s (Hoell et al. 2015a). The anomalous high pressure shown in the 200-hPa geopotential height anomaly field over southern Asia during 1975–2012 La Niña is consistent with the strong simulated negative precipitation anomalies during that same time, where the interaction of such a high pressure with the midlatitude jet produces anomalous descent (Hoell et al. 2015a).

By contrast, the global SST and simulated 200-hPa geopotential height anomalies during 1901–37 and 1938–74 La Niña are much different than those during 1975–2012 La Niña (Fig. 12). The 1901–74 La Niña SST anomalies do not exhibit the sharp difference between the cool central tropical Pacific Ocean and the warm western tropical Pacific Ocean (~0.8°C) when compared with 1975–2012 La Niña (~1.5°C). The 1901–74 La Niña SST anomalies are cooler globally than during 1975–2012 La Niña, except for the central tropical Pacific Ocean, which has approximately the same magnitude SST anomalies. There is very little structure in the global 200-hPa geopotential height anomalies during 1901–74 La Niña when compared with 1975–2012 La Niña. This is especially true over the entire Northern Hemisphere, and in particular over the Mediterranean region and across Asia, where 1901–74 La Niña events are related to weak zonal and meridional 200-hPa geopotential height anomaly gradients. The weak 200-hPa geopotential height anomaly gradients during 1901–74 La Niña over western Asia in part explain the weak

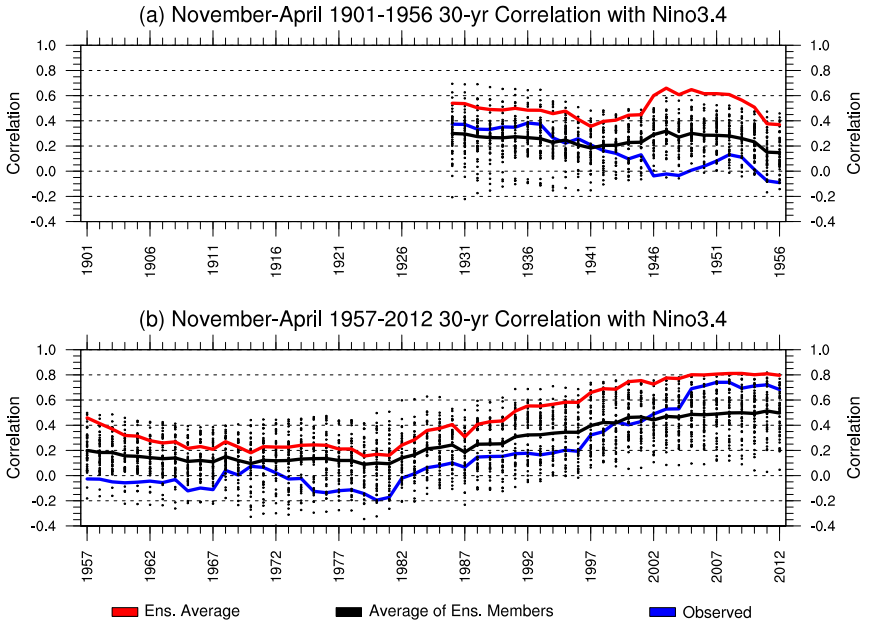

FIG. 10. November–April 30-yr end point correlation of the observed Niño-3.4 index and areally averaged southwest Asia precipitation resolved by observation (blue line), simulated ensemble average (red line), simulated ensemble members (black dots), and average of the simulated ensemble members (black line).

southwest Asia precipitation anomaly response relative to 1975–2012 La Niña.

El Niño is on average related to broadly similar November–April southwest Asia precipitation patterns and magnitudes across 1901–37, 1938–74, and 1975–2012 (Fig. 13). El Niño events during the three periods analyzed are related to statistically significant regionwide above-average southwest Asia precipitation. One difference in southwest Asia precipitation among the three periods analyzed is that the anomalously wet conditions throughout the region have stronger magnitudes during earlier El Niño events (1901–37) when compared with later El Niño events (1975–2012), particularly over Saudi Arabia, Iraq, and Iran. The PDFs of areally averaged southwest Asia precipitation during El Niño of the three periods analyzed indicate significant increases in the likelihood of regionwide wet conditions relative to ENSO neutral precipitation. However, precipitation during recent El Niño events indicates a shift toward drier conditions, in both the maximum likelihoods and the tails of the distribution, when compared with precipitation during earlier El Niño events.

The similar Southwest Asia precipitation patterns and magnitudes during El Niño of 1975–2012, 1938–74, and 1901–37 are explained to first order by similar global 200-hPa geopotential height and SST anomaly structures (Fig. 14). El Niño–related SST anomalies during all three periods are characterized by an SST anomaly contrast between the central and western tropical Pacific Ocean in excess of 1°C. There is no apparent change in the magnitude of the anomalous zonal SST gradient between the Indo-western and central Pacific Ocean during El Niño across 1901–2012, in stark contrast with La Niña (cf. Figs. 14 and 12). The magnitude of the anomalous zonal Pacific SST

TABLE 2. List of El Niño and La Niña events. El Niño (La Niña) events are defined to occur when the November–April average Niño-3.4 index exceeds (falls below) 0.5°C (−0.5°C)

November–April	El Niño	La Niña
1901–37	1902/03, 1904/05, 1905/06, 1911/12, 1913/14, 1918/19, 1923/24, 1925/26, and 1930/31	1903/04, 1908/09, 1909/10, 1910/11, 1916/17, 1917/18, 1922/23, 1924/25, and 1933/34
1938–74	1939/40, 1940/41, 1941/42, 1957/58, 1963/64, 1965/66, 1968/69, 1969/70, and 1972/73	1938/39, 1942/43, 1949/50, 1950/51, 1954/55, 1955/56, 1964/65, 1967/68, 1970/71, 1971/72, 1973/74, and 1974/75
1975–2012	1976/77, 1977/78, 1982/83, 1986/87, 1987/88, 1991/92, 1994/95, 1997/98, 2002/03, 2004/05, 2006/07, and 2009/10	1975/76, 1983/84, 1984/85, 1988/89, 1995/96, 1998/99, 1999/2000, 2000/01, 2005/06, 2007/08, 2008/09, 2010/11, and 2011/12

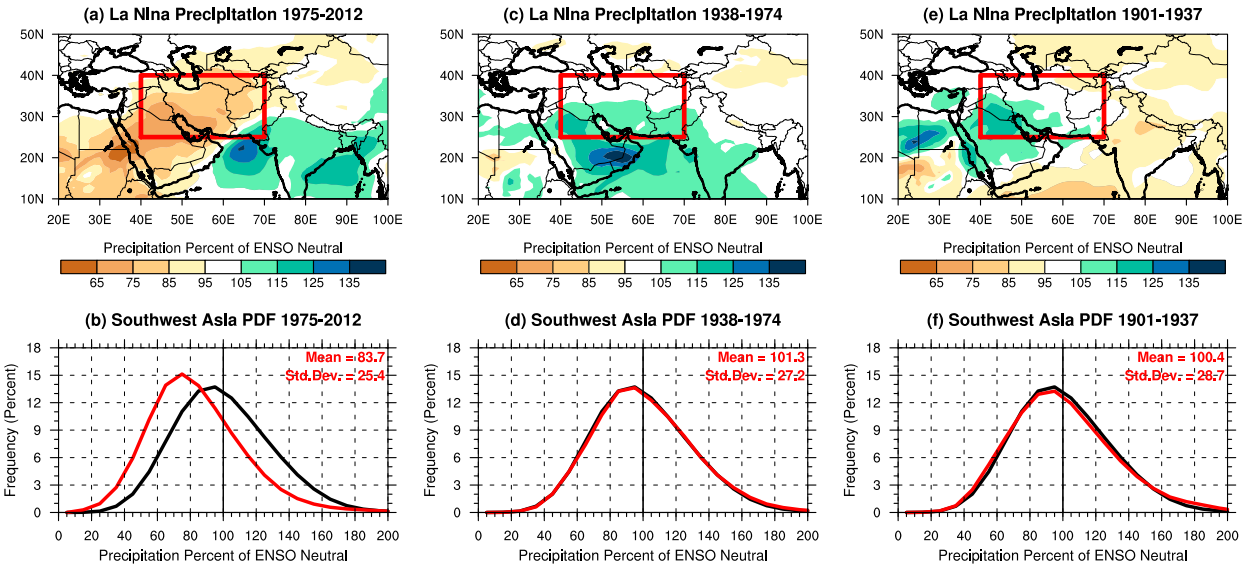

FIG. 11. (a),(c),(e) Simulated La Niña November–April precipitation percent of ENSO neutral and (b),(d),(f) southwest Asia PDF (red curve) during (left) 1975–2012, (center) 1938–74, and (right) 1901–37. The ENSO neutral southwest Asia precipitation PDFs during the labeled time period are shown in black. Spatial precipitation is significant at $p < 0.10$ using the two-sided Student's t test.

gradient during El Niño appears to remain consistent through time due to similar rates of warming in the western and central Pacific Ocean during El Niño of 1901–2012.

The structure of 200-hPa geopotential height anomalies over the Northern Hemisphere are similar across El Niño events of the three periods despite the noticeable increase in geopotential heights through time (Fig. 14, contours). During El Niño of 1975–2012, 1938–74, and 1901–37, southwest Asia is consistently located in a minimum of geopotential height anomalies, which to first order explain the regional precipitation increases relative to ENSO neutral. Furthermore, a characteristic response to El Niño, the tropical Northern Hemisphere pattern (Mo and Livezey 1986), is prominent during El Niño of all periods considered.

b. *SST and long-term southwest Asia precipitation declines*

The decline in western southwest Asia precipitation surpluses during El Niño in recent decades motivate us to examine whether the regional precipitation declines also occur during ENSO neutral conditions. We therefore assess the temporal changes in southwest Asia precipitation during ENSO neutral conditions, when the Niño-3.4 index falls between −0.5° and 0.5°C, across the three time periods of nearly equal length: 1901–37, 1938–74, and 1975–2012. These three roughly 36-yr time periods are analyzed to provide a large enough sample size in which to track the changing relationships between SSTs and southwest Asia precipitation. Southwest Asia climate is examined in terms of spatial precipitation and PDFs of areally averaged regional precipitation. Results are displayed as anomalies relative to 1901–2012 ENSO neutral conditions to assess the changes in a historical context, and to neglect the biases that ENSO may introduce.

The contrast between 1938–74 and 1975–2012 precipitation anomalies reveals a trend toward drier conditions over western southwest Asia and a trend toward wetter conditions over eastern southwest Asia during ENSO neutral conditions (Fig. 15). There is minimal departure from the long-term average precipitation during 1901–37 ENSO neutral over southwest Asia. The 1975–2012 ENSO neutral precipitation anomaly, with drying over Iran, Iraq, and Saudi Arabia and wetting over Pakistan and Afghanistan, closely resembles the second principal component of southwest Asia precipitation in observations (Fig. 3c), simulations from each model (Figs. 4d–f), and the ensemble average of all models (Fig. 3d). By contrast, the 1938–74 ENSO neutral precipitation anomaly pattern is the inverse of the 1975–2012 ENSO neutral precipitation anomaly pattern, but with weaker magnitudes of the regional precipitation anomalies. It is therefore plausible to conclude that a long-term change in southwest Asia precipitation is a prominent component of the regional precipitation variability, and is expressed as a west–east precipitation dipole across the region.

The PDFs of ENSO neutral subregional southwest Asia precipitation during 1938–74 and 1975–2012 are examined through a separation of southwest Asia into western and eastern halves, with the 55°E line of

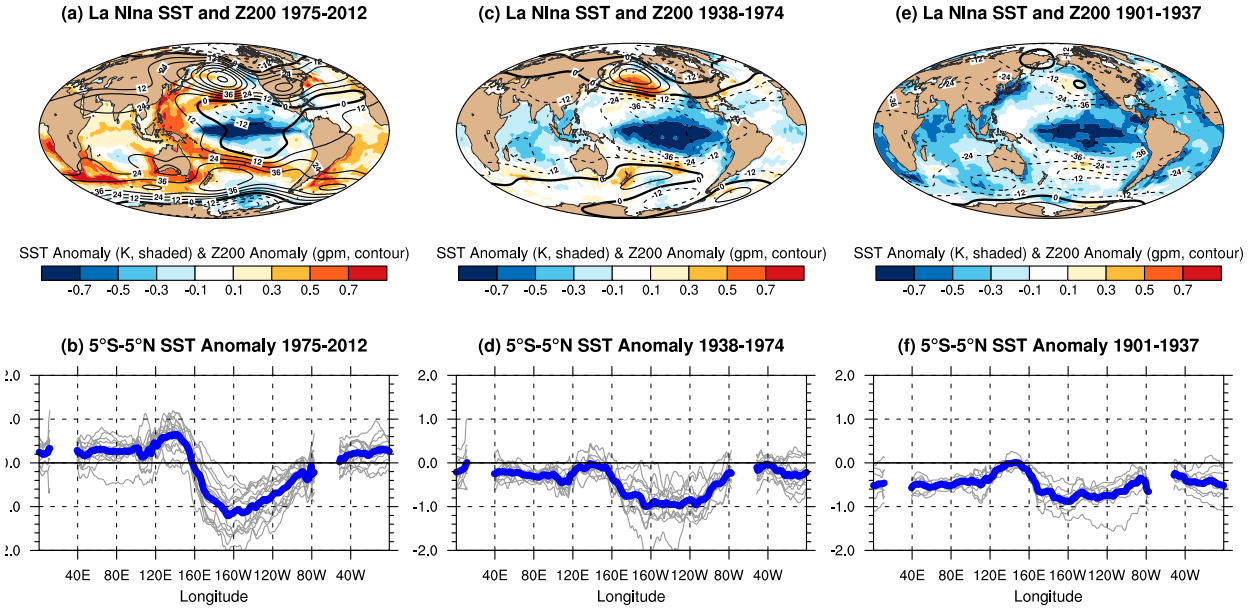

FIG. 12. November–April La Niña (a),(c),(e) average SST anomaly and simulated average 200-hPa geopotential height anomaly and (b),(d),(f) 5°S–5°N average SST anomaly for each event (gray) and for the average of all events (blue) during (left) 1975–2012, (center) 1938–74, and (right) 1901–37. Spatial SST anomalies are significant at $p < 0.10$ using the two-sided Student's t test.

longitude serving as the barrier between the two subregions. Over western southwest Asia, there is a noticeable shift in the PDF to drier conditions in the maximum likelihoods and wet tails of the precipitation distribution between the periods of 1975–2012 and 1938–74 (cf. Figs. 15b,e). By contrast, over eastern southwest Asia, there is a shift in the maximum likelihood to wetter conditions and a minimal shift of the wet and dry tails of the PDFs to wetter conditions between the periods of 1975–2012 and 1938–74 (cf. Figs. 15c,f).

SSTs and geopotential heights are analyzed to provide a first-order diagnosis of the potential drivers of ENSO neutral southwest Asia precipitation changes between 1938–74 and 1975–2012 (Fig. 16). The change in SST between 1938–74 and 1975–2012 shows prominent warming of the Indo-western Pacific Ocean and comparably much weaker warming of the central and

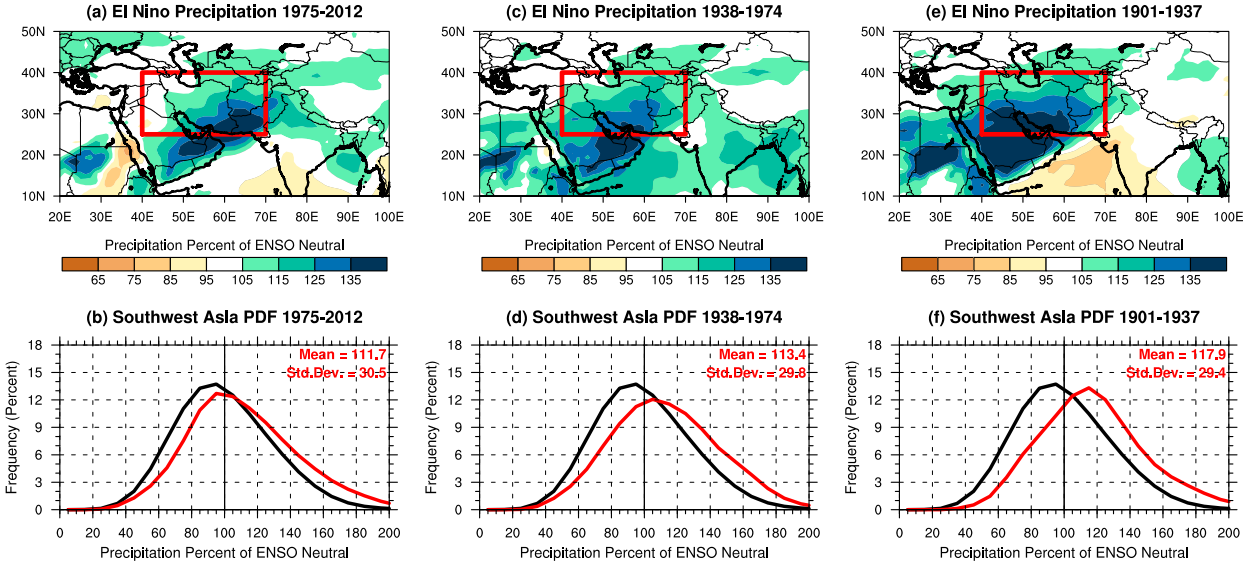

FIG. 13. As in Fig. 11, but for El Niño.

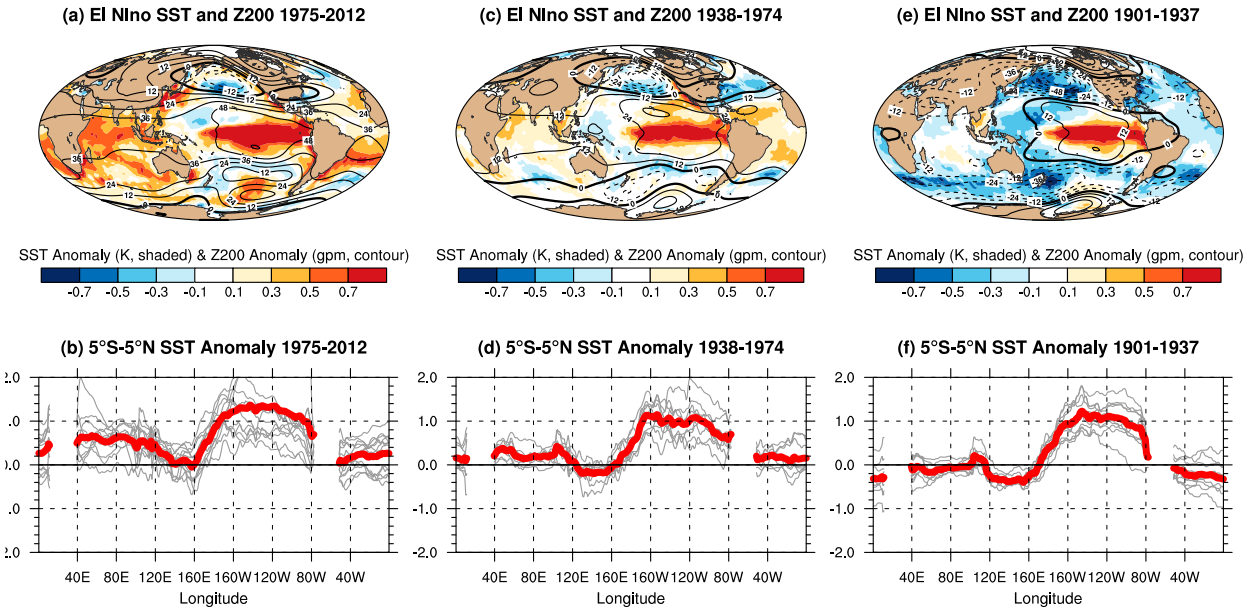

FIG. 14. As in Fig. 12, but for El Niño; average of all events is shown in red.

eastern Pacific Ocean (cf. Figs. 16a,b). Equatorial averages of ENSO neutral SST during 1975–2012 highlight the preferred warming of Indo-western Pacific SST, and the enhanced zonal SST gradient between the Indo-western and central Pacific produced by such enhanced warming. The similarly enhanced zonal SST gradient during La Niña of 1975–2012 (cf. Figs. 12b and 16b) is also linked to reduced western southwest Asia precipitation (cf. Figs. 15a and 11a), which highlights that such an enhanced zonal gradient may indeed be important to the region's precipitation.

The overall increases in global SSTs occur simultaneously with increases in global geopotential height anomalies during 1938–74 and 1975–2012 (Fig. 16). During 1975–2012, the rapid increases in tropical Indo-western Pacific SST are associated with a northward expanse of the 18-gpm contour from the tropics into southern Asia, which in turn increases in the meridional gradients of geopotential height anomalies over southwest Asia. There is a local maximum of geopotential height anomalies over the southern Arabian Peninsula and Arabian Sea, which has the effect of pushing the subtropical jet stream northward (not shown), thereby reducing precipitation over westernmost southwest Asia (Fig. 15a).

5. Summary and discussion

The long-term variability of November–April southwest Asia precipitation and its relationship with Pacific SST was examined using a large ensemble of atmospheric model simulations forced by 1901–2012 time-varying boundary conditions. Previous studies have identified the links between November–April southwest Asia precipitation and SSTs associated with ENSO and warming of Pacific SSTs (Barlow et al. 2002, 2016; Mariotti 2007; Hoell and Funk 2013; Hoell et al. 2013, 2014b, 2015a,b, 2017; Cannon et al. 2017). However, because of data limitations, these studies have focused primarily on the mid twentieth century and later. Here, a 43-member ensemble of atmospheric model simulations is validated against observations during the best-observed 1960–2005 period and then used to investigate the causality, sensitivity, and changing temporal relationships of southwest Asia precipitation to SST patterns associated with ENSO and warming of Pacific SST.

Three atmospheric models were employed in this study: 14 simulations from the NCAR CAM5, 17 simulations from the GFDL AM3, and 12 simulations from the NASA GEOS-5. The models were forced by prescribed 1901–2012 time-varying boundary conditions, which include SST, sea ice concentrations, greenhouse gases, and ozone. Each ensemble member has different weather variability owing to their initialization from different atmospheric states. The atmospheric models provide a reasonable simulation of November–April southwest Asia 1960–2005 precipitation in terms of precipitation means, the leading patterns of precipitation variability, the global SST, and atmospheric circulation patterns associated with the leading patterns of precipitation variability and temporal precipitation variability.

The ability of the atmospheric models to capture realistic variability and mean November–April southwest

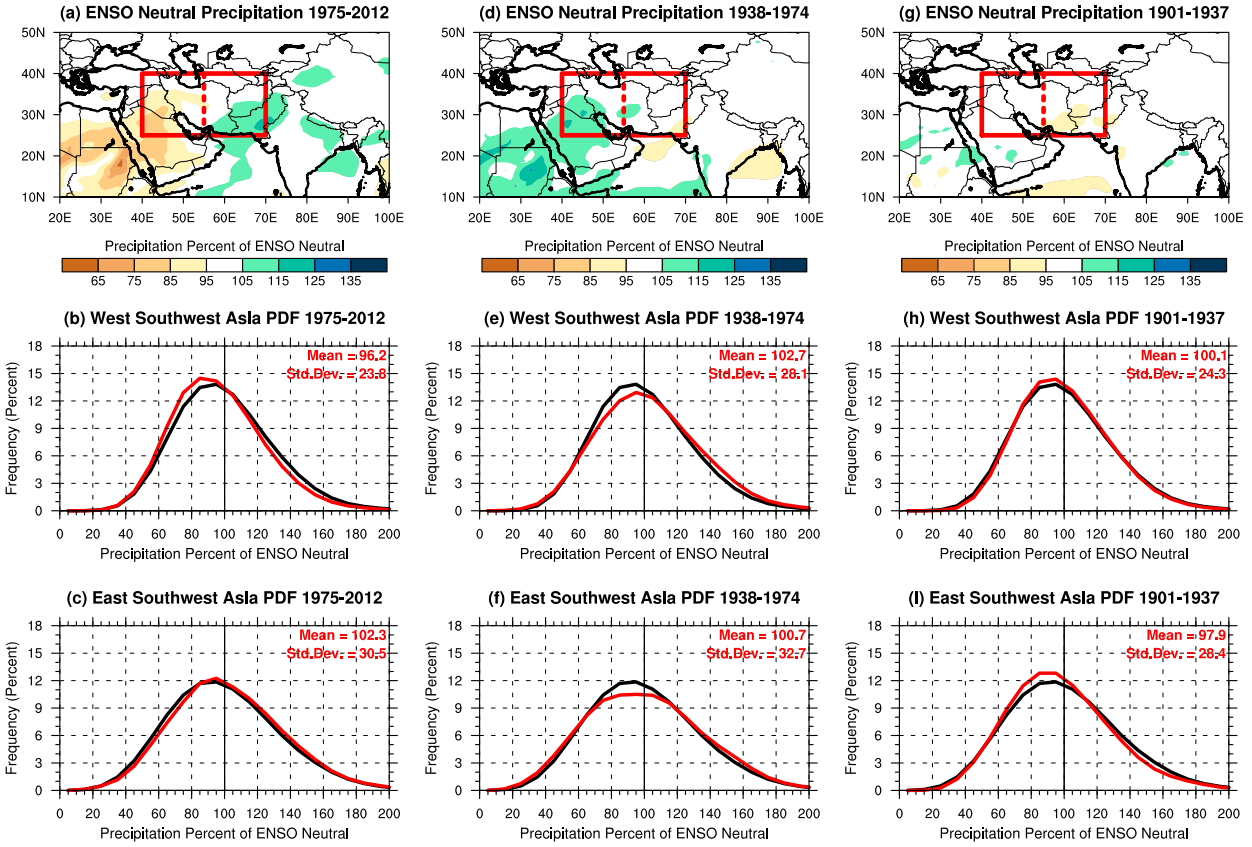

FIG. 15. (a),(d),(g) Simulated ENSO neutral November–April precipitation percent of 1901–2012 ENSO neutral and (b),(e),(h) areally averaged western southwest Asia PDF (red curve), and (c),(f),(i) areally averaged easternmost southwest Asia PDF (red curve) during (left) 1975–2012, (center) 1938–74, and (right) 1901–37. The 1901–2012 ENSO neutral precipitation PDF is shown in black. Spatial precipitation is significant at $p < 0.10$ using the two-sided Student's t test.

Asia precipitation has important positive implications for seasonal climate prediction of precipitation throughout the region. Each of the atmospheric models employed in this manuscript serves as the atmospheric component of a coupled climate model that is part of the North American Multimodel Ensemble phase II (Kirtman et al. 2014; CPC 2014). The ability of the atmospheric models to simulate appropriate southwest Asia precipitation responses to ENSO, in particular, certainly improves confidence in the robustness of the forecasts generated by coupled climate models on seasonal time scales.

Each of the models indicates that the leading mode of November–April southwest Asia precipitation variability is related to ENSO. However, the coupling between ENSO and southwest Asia precipitation during 1901–2012 varied throughout time. Using the Niño-3.4 index as an indicator of ENSO, the average 30-yr end point correlations between the Niño-3.4 index and simulated southwest Asia precipitation for each ensemble varied from 0.3 prior to the 1950s, to 0.10 in the 1970s, and to 0.50 in the early 2000s. To that end, the period 1901–2012 was separated into three periods of nearly equal size, and southwest Asia precipitation, SSTs, and the hemispheric circulation were analyzed during El Niño and La Niña. This separation allowed us to examine the physical changes in the relationship between ENSO's two phases and southwest Asia precipitation.

In aggregate, November–April southwest Asia precipitation during 1975–2012 La Niña was below average regionwide. By contrast, aggregate November–April southwest Asia precipitation during 1901–74 La Niña was not materially different from the long-term ENSO neutral average. The variable behavior of southwest Asia precipitation during La Niña across the three time periods considered help to explain the poor correlations between the Niño-3.4 index and southwest Asia precipitation prior to the 1970s. The differences in southwest Asia precipitation between La Niña of 1975–2012, 1938–74, and 1901–37 are related to different global atmospheric circulations. Strong anomalies and gradients in the 200-hPa geopotential height field are related to 1975–2012 La Niña, highlighted by high pressure over

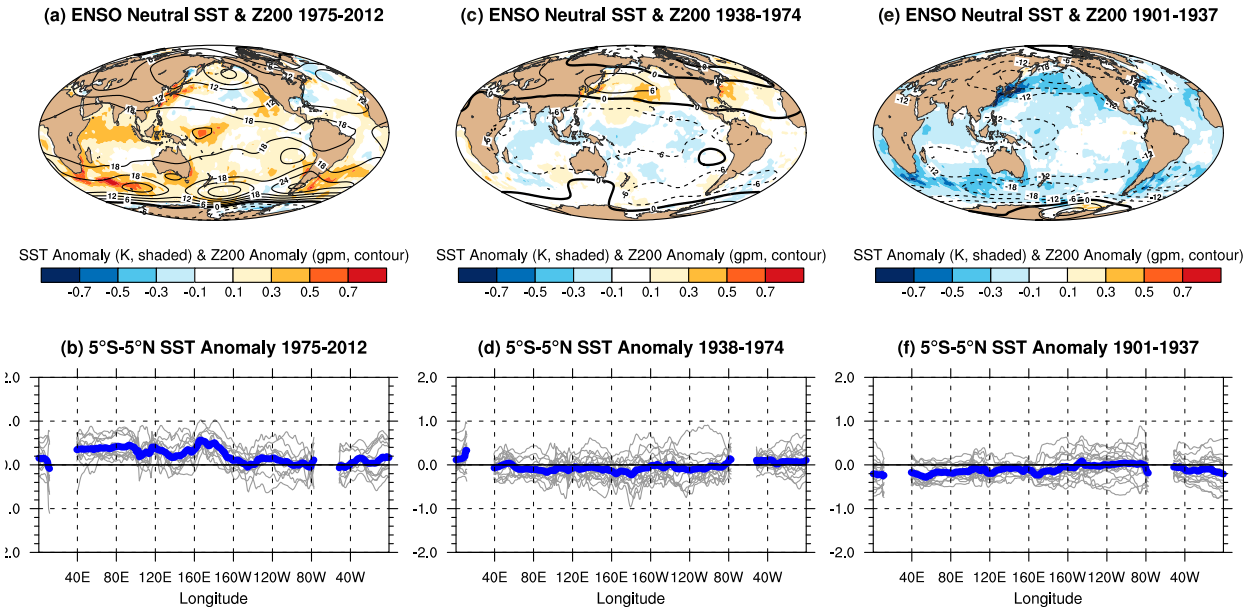

FIG. 16. November–April ENSO neutral (a),(c),(e) average SST anomaly and simulated average 200-hPa geopotential height anomaly and (b),(d),(f) 5°S–5°N average SST anomaly for each event (gray) and for the average of all events (blue) during (left) 1975–2012, (center) 1938–74, and (right) 1901–37. Spatial SST anomalies are significant at $p < 0.10$ using the two-sided Student's t test.

southwest Asia. By contrast, there is very little structure in the global 200-hPa geopotential height anomalies during 1901–74 La Niña when compared with 1975–2012 La Niña.

The average tropical Pacific SST anomaly patterns during La Niña of 1975–2012, 1938–74, and 1901–37 are quite different, which to first order explains the differences in the November–April southwest Asia precipitation and hemispheric circulation. The average SST anomalies during La Niña of 1975–2012 are characterized by a sharp contrast between the central and western tropical Pacific Ocean in excess of 1.5°C. By contrast, the average 1901–74 La Niña SST anomalies are missing the sharp difference between the cool central tropical Pacific Ocean and the warm western tropical Pacific Ocean (~0.8°C) when compared with 1975–2012 La Niña.

In aggregate, El Niño across 1901–37, 1938–74, and 1975–2012 were related with broadly similar November–April southwest Asia precipitation patterns and magnitudes. One difference in southwest Asia precipitation between the three periods analyzed is that the anomalously wet conditions throughout the region have stronger magnitudes during earlier El Niño events (e.g., 1901–37) when compared with later El Niño events (e.g., 1975–2012), particularly over Saudi Arabia, Iraq, and Iran. The similar southwest Asia precipitation patterns and magnitudes during El Niño across the three periods considered also related similar global 200-hPa geopotential height and SST anomalies. El Niño–related SST anomalies during all three periods are characterized by an SST anomaly contrast between the central and western tropical Pacific Ocean in excess of 1°C. The structure of 200-hPa geopotential height anomalies over the Northern Hemisphere is similar across El Niño events of the three periods despite the noticeable increase in geopotential heights.

The common oceanic feature related with strong regionwide November–April southwest Asia precipitation anomalies during both El Niño and La Niña is the SST anomaly contrast between the western and central tropical Pacific Oceans, identified as the western Pacific gradient by Hoell and Funk (2013). Hoell and Funk (2013) found in observations that the magnitude of the western Pacific gradient has increased during La Niña in the latter part of the twentieth century, and that strong drought over southwest Asia was related to such a gradient enhancement. The results presented herein, based upon atmospheric model simulations forced by observed time-varying boundary conditions, thereby affirm the observational results of Hoell and Funk (2013). During both El Niño and La Niña, an SST anomaly contrast between the western and central tropical Pacific Ocean of greater than 1°C in magnitude is related to significant southwest Asia precipitation anomalies. It so happened that such an SST anomaly contrast occurred in aggregate during El Niño of all of the periods considered, whereas such an SST anomaly contrast only occurred in aggregate during 1975–2012 La Niña. Future studies should therefore focus on the

sensitivity of southwest Asia climate to variations in the magnitude of the contrast between the tropical western and central Pacific Ocean.

The observed warming of the western Pacific Ocean relative to the central Pacific Ocean during the twentieth and early twenty-first centuries, identified by Compo and Sardeshmukh (2010) and Solomon and Newman (2012), appears to have increased the magnitude of the SST contrast between the western and central tropical Pacific Ocean during La Niña. However, the observed warming of the western Pacific Ocean relative to the central Pacific Ocean during the twentieth and early twenty-first centuries only appears to have a marginal effect on the magnitude of the SST contrast between the western and central tropical Pacific Ocean during El Niño. During El Niño, the effect of the long-term changes reduces the west–east contrast in SST anomalies over the Pacific Ocean, but not substantially so during the twentieth and twenty-first centuries. Therefore, the effect of the long-term changes in Pacific SST appear to have a tangible influence during La Niña, and a much weaker influence during El Niño, as they relate to the forcing of November–April southwest Asia precipitation.

The long-term changes in November–April southwest Asia precipitation during El Niño and La Niña motivated us to examine the long-term southwest Asia precipitation changes during ENSO neutral conditions. The contrast between 1938–74 and 1975–2012 southwest Asia ENSO neutral precipitation anomalies reveals a trend toward drier conditions over western southwest Asia and a trend toward wetter conditions over eastern southwest Asia. There is minimal departure from the long-term average precipitation during 1901–37 ENSO neutral over southwest Asia. The contrast between 1975–2012 and 1938–74 southwest Asia ENSO neutral precipitation is expressed as a west–east precipitation dipole across the region, similar to the second principal component of southwest Asia precipitation. Therefore, it is plausible to conclude that a long-term change in southwest Asia precipitation is a prominent component of the regional precipitation variability.

The concomitant SST changes between 1938–74 and 1975–2012 reveal prominent warming of the Indo-western Pacific Ocean and comparably much weaker warming of the central and eastern Pacific Ocean. The long-term SST changes thereby enhance the west–east contrast in SST anomalies over the Pacific Ocean, similar to La Niña of 1975–2012. Therefore, the long-term Pacific SST changes also appear to have an important drying effect on November–April southwest Asia ENSO neutral precipitation.

Significant changes in November–April southwest Asia precipitation during El Niño, La Niña, and ENSO neutral are all linked to a strong SST anomaly contrast between the western and central Pacific Ocean in time-varying model simulations and observations. It is therefore important to better understand the direct sensitivity of southwest Asia climate to the SST anomaly contrast between the western and central Pacific Ocean.

Finally, the fact that important changes in precipitation and SST influence are simulated by models in the pre-1960 period when observations are extremely limited highlights the need for more efforts to obtain and process observational data for the region, integrate it with modeling data, investigate the influence of changes in sampling, and provide uncertainty estimates.

Acknowledgments. The authors thank Quan Xiao-Wei for performing the CAM5 and AM3 simulations and Hailan Wang for providing the GEOS-5 simulations. The authors also thank three anonymous reviewers for constructive comments. The authors are grateful for support from the Famine Early Warning Systems Network.

REFERENCES

Aizen, E. M., V. B. Aizen, J. M. Melack, T. Nakamura, and T. Ohta, 2001: Precipitation and atmospheric circulation patterns at mid-latitudes of Asia. *Int. J. Climatol.*, **21**, 535–556, doi:10.1002/joc.626.

Barlow, M., H. Cullen, and B. Lyon, 2002: Drought in central and southwest Asia: La Niña, the warm pool, and Indian Ocean precipitation. *J. Climate*, **15**, 697–700, doi:10.1175/1520-0442(2002)015<0697:DICASA>2.0.CO;2.

——, M. Wheeler, B. Lyon, and H. Cullen, 2005: Modulation of daily precipitation over southwest Asia by the Madden–Julian oscillation. *Mon. Wea. Rev.*, **133**, 3579–3594, doi:10.1175/MWR3026.1.

——, B. Zaitchik, S. Paz, E. Black, J. Evans, and A. Hoell, 2016: A review of drought in the Middle East and southwest Asia. *J. Climate*, **29**, 8547–8574, doi:10.1175/JCLI-D-13-00692.1.

Cannon, F., L. M. V. Carvalho, C. Jones, A. Hoell, J. Norris, G. N. Kiladis, and A. A. Tahir, 2017: The influence of tropical forcing on extreme winter precipitation in the western Himalaya. *Climate Dyn.*, **48**, 1213–1232, doi:10.1007/s00382-016-3137-0.

Compo, G. P., and P. D. Sardeshmukh, 2010: Removing ENSO-related variations from the climate record. *J. Climate*, **23**, 1957–1978, doi:10.1175/2009JCLI2735.1.

——, and Coauthors, 2011: The Twentieth Century Reanalysis Project. *Quart. J. Roy. Meteor. Soc.*, **137**, 1–28, doi:10.1002/qj.776.

CPC, 2014: NMME phase-II data plan. Climate Prediction Center. [Available online at http://www.cpc.ncep.noaa.gov/products/ctb/nmme/NMME-PhaseII-DataPlan-27May.pdf.]

Cullen, H. M., and P. B. deMenocal, 2000: North Atlantic influence on Tigris–Euphrates streamflow. *Int. J. Climatol.*, **20**, 853–863, doi:10.1002/1097-0088(20000630)20:8<853::AID-JOC497>3.0.CO;2-M.

——, A. Kaplan, P. A. Arkin, and P. B. deMenocal, 2002: Impact of the North Atlantic Oscillation on Middle Eastern climate and streamflow. *Climatic Change*, **55**, 315–338, doi:10.1023/A:1020518305517.

Dai, A., 2013: The influence of the inter-decadal Pacific oscillation on US precipitation during 1923–2010. *Climate Dyn.*, **41**, 633–646, doi:10.1007/s00382-012-1446-5.

Donner, L. J., and Coauthors, 2011: The dynamical core, physical parameterizations, and basic simulation characteristics of the atmospheric component AM3 of the GFDL global coupled model CM3. *J. Climate*, **24**, 3484–3519, doi:10.1175/2011JCLI3955.1.

Hoell, A., and C. Funk, 2013: The ENSO-related west Pacific sea surface temperature gradient. *J. Climate*, **26**, 9545–9562, doi:10.1175/JCLI-D-12-00344.1.

——, M. Barlow, and R. Saini, 2013: Intraseasonal and seasonal-to-interannual Indian Ocean convection and hemispheric teleconnections. *J. Climate*, **26**, 8850–8867, doi:10.1175/JCLI-D-12-00306.1.

——, C. Funk, and M. Barlow, 2014a: The regional forcing of Northern Hemisphere drought during recent warm tropical west Pacific Ocean La Niña events. *Climate Dyn.*, **42**, 3289–3311, doi:10.1007/s00382-013-1799-4.

——, ——, and ——, 2014b: La Niña diversity and northwest Indian Ocean Rim teleconnections. *Climate Dyn.*, **43**, 2707–2724, doi:10.1007/s00382-014-2083-y.

——, ——, and ——, 2015a: The forcing of southwestern Asia teleconnections by low-frequency sea surface temperature variability during boreal winter. *J. Climate*, **28**, 1511–1526, doi:10.1175/JCLI-D-14-00344.1.

——, S. Shukla, M. Barlow, F. Cannon, C. Kelley, and C. Funk, 2015b: The forcing of monthly precipitation variability over southwest Asia during the boreal cold season. *J. Climate*, **28**, 7038–7056, doi:10.1175/JCLI-D-14-00757.1.

——, C. Funk, M. Barlow, and F. Cannon, 2017: Extreme drought over southwest Asia: A physical model. *Climate Extremes: Mechanisms and Potential Prediction*, S. Wang, C. Funk, and R. Gillies, Eds., American Geophysical Union, in press.

Hurrell, J. W., J. J. Hack, D. Shea, J. M. Caron, and J. Rosinski, 2008: A new sea surface temperature and sea ice boundary dataset for the Community Atmosphere Model. *J. Climate*, **21**, 5145–5153, doi:10.1175/2008JCLI2292.1.

Kirtman, B. P., and Coauthors, 2014: The North American Multimodel Ensemble: Phase-1 seasonal-to-interannual prediction; phase-2 toward developing intraseasonal prediction. *Bull. Amer. Meteor. Soc.*, **95**, 585–601, doi:10.1175/BAMS-D-12-00050.1.

Krichak, O. S., P. Kishcha, and P. Alpert, 2002: Decadal trends of main Eurasian oscillations and the eastern Mediterranean precipitation. *Theor. Appl. Climatol.*, **72**, 209–220, doi:10.1007/s007040200021.

Lamarque, J.-F., and Coauthors, 2010: Historical (1850–2000) gridded anthropogenic and biomass burning emissions of reactive gases and aerosols: Methodology and application. *Atmos. Chem. Phys.*, **10**, 7017–7039, doi:10.5194/acp-10-7017-2010.

——, and Coauthors, 2011: Global and regional evolution of short-lived radiatively-active gases and aerosols in the representative concentration pathways. *Climatic Change*, **109**, 191–212, doi:10.1007/s10584-011-0155-0.

Mann, M. E., 2002: Large-scale climate variability and connections with the Middle East in past centuries. *Climatic Change*, **55**, 287–314, doi:10.1023/A:1020582910569.

Mantua, N. J., S. R. Hare, Y. Zhang, J. M. Wallace, and R. C. Francis, 1997: A Pacific interdecadal climate oscillation with impacts on salmon production. *Bull. Amer. Meteor. Soc.*, **78**, 1069–1079, doi:10.1175/1520-0477(1997)078<1069:APICOW>2.0.CO;2.

Mariotti, A., 2007: How ENSO impacts precipitation in southwest central Asia. *Geophys. Res. Lett.*, **34**, L16706, doi:10.1029/2007GL030078.

Meinshausen, M., and Coauthors, 2011: The RCP greenhouse gas concentrations and their extensions from 1765 to 2300. *Climatic Change*, **109**, 213–241, doi:10.1007/s10584-011-0156-z.

Mo, K. C., and R. E. Livezey, 1986: Tropical–extratropical geopotential height teleconnections during the Northern Hemisphere winter. *Mon. Wea. Rev.*, **114**, 2488–2515, doi:10.1175/1520-0493(1986)114<2488:TEGHTD>2.0.CO;2.

Molod, A., L. Takacs, M. Suarez, J. Bacmeister, I. Song, and A. Eichmann, 2012: The GEOS-5 Atmospheric General Circulation Model: Mean climate and development from MERRA to Fortuna. NASA Tech. Rep. Series on Global Modeling and Data Assimilation, NASA/TM-2012-104606, Vol. 28, 117 pp. [Available online at https://gmao.gsfc.nasa.gov/pubs/docs/tm28.pdf.]

Nazemosadat, M. J., and H. Ghaedamini, 2010: On the relationships between the Madden–Julian oscillation and precipitation variability in southern Iran and the Arabian Peninsula: Atmospheric circulation analysis. *J. Climate*, **23**, 887–904, doi:10.1175/2009JCLI2141.1.

Neale, R. B., and Coauthors, 2012: Description of the NCAR Community Atmosphere Model (CAM 5.0). NCAR Tech. Note NCAR/TN-486+STR, 274 pp. [Available online at http://www.cesm.ucar.edu/models/cesm1.0/cam/docs/description/cam5_desc.pdf.]

Schneider, U., A. Becker, P. Finger, A. Meyer-Christoffer, M. Ziese, and B. Rudolf, 2014: GPCC's new land surface precipitation climatology based on quality-controlled in situ data and its role in quantifying the global water cycle. *Theor. Appl. Climatol.*, **115**, 15–40, doi:10.1007/s00704-013-0860-x.

Schubert, S., and Coauthors, 2009: A U.S. CLIVAR project to assess and compare the responses of global climate models to drought-related SST forcing patterns: Overview and results. *J. Climate*, **22**, 5251–5272, doi:10.1175/2009JCLI3060.1.

——, H. Wang, R. D. Koster, M. J. Suarez, and P. Ya. Groisman, 2014: Northern Eurasian heat waves and droughts. *J. Climate*, **27**, 3169–3207, doi:10.1175/JCLI-D-13-00360.1.

Solomon, A., and M. Newman, 2012: Reconciling disparate twentieth-century Indo-Pacific ocean temperature trends in the instrumental record. *Nat. Climate Change*, **2**, 691–699, doi:10.1038/nclimate1591.

Syed, S. F., F. Giorgi, S. J. Pal, and P. M. King, 2006: Effect of remote forcings on the winter precipitation of central southwest Asia. Part 1: Observations. *Theor. Appl. Climatol.*, **86**, 147–160, doi:10.1007/s00704-005-0217-1.